Journal of Power Sources 246 (2014) 659–666

Contents lists available at ScienceDirect

Journal of Power Sources

journal homepage: www.elsevier.com/locate/jpowsour

Short communication

Pulse electrodeposition to prepare core–shell structured AuPt@Pd/C catalyst for formic acid fuel cell application

Xueyi Lu, Fan Luo, Huiyu Song, Shijun Liao*, Hualing Li

Key Laboratory for Fuel Cell Technology of Guangdong Province, School of Chemistry and Chemical Engineering, South China University of Technology, Guangzhou 510641, China

HIGHLIGHTS

- The particle size of Au could be reduced by the addition of small amount of Pt.
- A core–shell catalyst was prepared by a facile pulse electrodeposition method.
- The catalyst exhibits excellent activity towards the oxidation of formic acid.

ARTICLE INFO

Article history:
Received 20 April 2013
Received in revised form
1 August 2013
Accepted 1 August 2013
Available online 15 August 2013

Keywords:
Core–shell structure
Catalyst
Electrodeposition
Formic acid
Electrooxidation

ABSTRACT

A novel core–shell structured AuPt@Pd/C catalyst for the electrooxidation of formic acid is synthesized by a pulse electrodeposition process, and the AuPt core nanoparticles are obtained by a $NaBH_4$ reduction method. The catalyst is characterized with X-ray powder diffraction and transmission electron microscopy, thermogravimetric analysis, cyclic voltammetry, CO stripping and X-ray photoelectron spectroscopy. The core–shell structure of the catalyst is revealed by the increase in particle size resulting from a Pd layer covering the AuPt core, and by a negative shift in the CO stripping peaks. The addition of a small amount of Pt improves the dispersion of Au and results in smaller core particles. The catalyst's activity is evaluated by cyclic voltammetry in formic acid solution. The catalyst shows excellent activity towards the anodic oxidation of formic acid, the mass activity reaches 4.4 A mg^{-1}_{Pd} and 0.83 A mg^{-1}_{metal}, which are 8.5 and 1.6 times that of commercial Pd/C. This enhanced electrocatalytic activity could be ascribed to the good dispersion of Au core particles resulting from the addition of Pt, as well as to the interaction between the Pd shell layer and the Au and Pt in the core nanoparticles.

1. Introduction

As the global energy crisis and various environmental problems have worsened in recent decades, fuel cells—energy conversion devices using hydrogen or low-molecular-weight alcohols as fuels [1]—have attracted increasing attention due to their numerous advantages, including high efficiency and environmental friendliness.

The direct formic acid fuel cell (DFAFC), which has developed rapidly in recent years, offers some notable advantageous features compared to other, currently more widely exploited, fuel cell types. For instance, it experiences lower crossover at the proton exchange membrane, has lower toxicity than methanol fuel cells, and yields high energy density and high open-circuit voltage [2–5]. Much work has been done to promote its performance since its emergence, and considerable progress in aspects of DFAFC research and engineering has been achieved [6,7]. However, its commercialization is still impeded by a few factors, among which the catalyst is the most vital one. The noble metals Pt and Pd have been widely used as fuel cell anode and cathode catalysts [8]. It is generally recognized that for formic acid oxidation, Pd shows better performance than Pt, because Pd can catalyze the electrooxidation of formic acid with greater resistance to CO than Pt [9–11], and it exhibits excellent initial activity even at low temperatures [12–14]. It is, however, essential to prepare porous Pd nanostructures containing nanosized particles on suitable substrates to exploit the high surface area to volume ratio and enhanced catalytic activity [15]. Therefore, the preparation of Pd nanostructures that are either solution based or coated on suitable substrates is of considerable interest among various research groups [13,15–19]. To date, a certain number of highly active Pd-based catalysts have been reported, including alloy and core–shell catalysts, such as PdIr/C [20], PdPt/C [21], PdAu [22], Ru@Pt_xPd_y [23], Pd@PtRu [24] and Pt_3Pb–Pt [25].

* Corresponding author. Fax: +86 20 87113586.
E-mail address: chsjliao@scut.edu.cn (S. Liao).

0378-7753/$ – see front matter © 2013 Elsevier B.V. All rights reserved.
http://dx.doi.org/10.1016/j.jpowsour.2013.08.004

Recently, the pulse electrodeposition method has been applied to the preparation of core–shell catalyst in our group, and this method can achieve a very thin shell, and can enhance the utilization of precious metal in shell layer greatly. In this background, we thought a core–shell palladium catalyst prepared by pulse electrodeposition might exhibit enhanced utilization and performance, even better stability than conventional Pd/C catalyst due to the synergetic effects existed between the Pd in shell layer and the metals in core. Considering the possible synergetic effect of Pd and Au, we chose Au as core material, unfortunately, it is very difficult to prepare a Au/C materials with small Au nanoparticles matching our desired size of 2–3 nm, no matter we used the colloidal method or impregnation–reduction method. It is interesting that if only a very little of platinum was added, the particle size of Au is decreased sharply to the range of our favorite size. Therefore, in this paper, a core–shell structured AuPt@Pd/C catalyst, in which the AuPt alloy was used as core, was prepared successfully by a pulse electrodeposition of a Pd layer on the Au nanoparticles, containing a small amount of Pt, which can improve Au dispersion and result in smaller nanoparticles of AuPt alloy [26]. It is interesting that this type of catalyst shows excellent activity towards the anodic oxidation of formic acid.

2. Experimental

2.1. Catalyst preparation

The core–shell structured AuPt@Pd/C catalyst was prepared using a two-stage process. In the first stage, AuPt alloy nanoparticles were prepared by a chemical reduction method. The typical preparation procedure was as follows. First, 22 mg PVA, used as a protecting agent, was added into 200 mL deionized water and heated to 90 °C for 20 min, then 2.0 mL $HAuCl_4$ solution (48.56 mmol L^{-1}) and 0.085 mL H_2PtCl_6 solution (38.62 mmol L^{-1}) were dropped into the above solution under vigorous stirring and ruby red sol was obtained. Next, 180 mg Vulcan XC-72R carbon was added to the sol under stirring for 6 h to immobilize the Au and Pt nanoparticles. Finally, the mixture was filtered and washed with deionized water and dried in a vacuum oven at 70 °C for 12 h. The content of AuPt alloy in AuPt/C is ca. 5% by weight, the theoretical atomic ratio of Au/Pt is 30, the actual atomic ratio is 28.5, measured by atomic adsorption spectrum (AAS) method.

Pd was deposited on the AuPt/C nanoparticles through a pulse electrodeposition process. 5 mg of this AuPt/C was put into 1 mL Nafion/ethanol (0.25 wt% Nafion) through ultrasonic dispersion to form a slurry, and 5 μl of this slurry was pipetted onto a 5 mm-diameter glassy carbon surface to function as a substrate. A $PdCl_2$ solution was used as the electrolyte, and a pulse electrodeposition procedure was applied to reduce the Pd onto the AuPt/C, yielding AuPt@Pd/C. The T_{on} (the time of connection) and T_{off} (the time of disconnection) in this work are 0.003 s and 0.015 s respectively. The theoretical deposited amount of Pd is calculated from the total deposition charge. And the actual deposited amount is determined by AAS analysis. It was found that the actual deposited amount is almost ten times of the theoretical deposited amount. Unless specified especially, the deposited amount in this paper is the actual amount analyzed by AAS, and the ratio of Au/Pd is also the actual ratio base on the AAS analysis results. And all the performance data presented in paper are calculated based on the actual deposited amount.

2.2. Catalyst characterization

X-ray powder diffraction (XRD) analysis was carried out with a Shimadzu XD-3A X-ray diffractometer (Japan) using filtered Cu Kα radiation at 35 kV and 30 mA. The 2θ region between 20° and 80° was explored at a scan rate of 4° min^{-1}. The average particle size of the catalyst was calculated using the Scherrer equation [27]:

$$d = \frac{0.9\lambda}{B_{2\theta}\cos\theta_{max}}$$

where λ is the wavelength of the X-ray (1.54056 Å), θ is the diffraction angle of the maximum of the peak, and $B_{2\theta}$ is the width of the peak at half-height.

Thermogravimetric analysis (TGA) was performed using a Q500 TGA analyzer (TA Instruments, UK) to examine the metal loading. The transmission electron microscope (TEM: JEOL JEM-2010HR, Japan) operated at 200 kV. For TEM analysis, the prepared catalyst was directly dissolved in ethanol using ultrasonic treatment, and a drop of catalyst powder suspension was applied to a wholly amorphous carbon film supported on a 3 mm diameter copper grid.

2.3. Electrochemical evaluation of the catalysts

The catalyst was evaluated with cyclic voltammetry (CV) and CO stripping using an Autolab electrochemical workstation at room temperature. The electrolytes were 0.5 M H_2SO_4 with or without 0.5 M HCOOH solutions. A conventional three-electrode electrochemical cell was used for the measurements. After Pd was reduced onto AuPt/C pipetted on the surface of a glassy carbon electrode, AuPt@Pd/C was prepared and the glassy carbon electrode acted as the working electrode. A Pt wire and an Ag/AgCl electrode (the latter saturated in 3 M NaCl) were used as the counter and reference electrodes, respectively. CO stripping voltammograms were measured in 0.5 M H_2SO_4. First, CO was purged into the H_2SO_4 solution for 10 min to allow the complete adsorption of CO onto the surface of the catalyst when the working electrode was kept at −0.1 mV vs. Ag/AgCl electrode. Then excess CO in the electrolyte was purged out with N_2 for 15 min. The amount of CO_{ad} was evaluated by integrating the CO_{ad} stripping peak. All the measurements were carried out at room temperature and the stable results were reported.

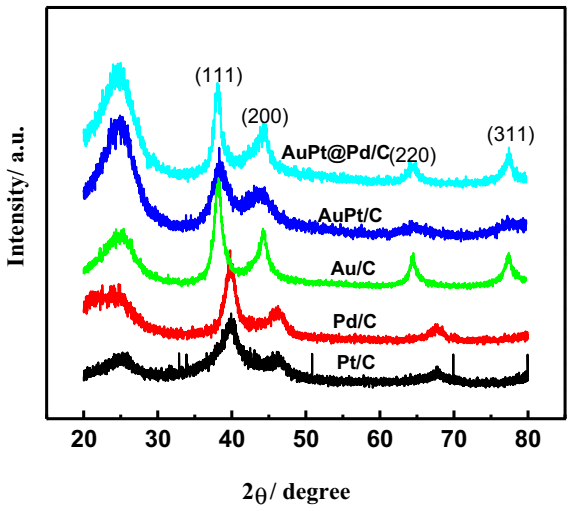

Fig. 1. X-ray diffraction patterns of Pt/C, Pd/C, Au/C, AuPt/C and AuPt@Pd/C.

3. Result and discussion

The XRD patterns shown in Fig. 1 clearly disclose the core–shell structure of AuPt@Pd/C. Comparing the patterns of Pt/C, Au/C and AuPt/C, we can see that AuPt/C possesses the structure of Au; thus, we suggest that the small amount of added Pt entered the Au lattice. Further, the pattern of AuPt@Pd/C is similar to that of AuPt/C, but not to that of Pd/C, and no obvious Pd diffraction peaks can be observed, revealing that the Pd may deposit on the structure of the AuPt nanoparticles instead of forming independent Pd nanoparticles.

As shown in Fig. 1, all the peaks of AuPt@Pd/C are clearly stronger than those of AuPt/C, which may be due to the deposition of Pd on the surface of the AuPt particles. The particle sizes, calculated from XRD data by Jade software, were 4.6 nm and 2.8 nm respectively. The size increase after pulse electrodeposition of Pd confirms the deposition of Pd on the surface of the AuPt particles. The thickness of the shell layer was ca. 0.9 nm.

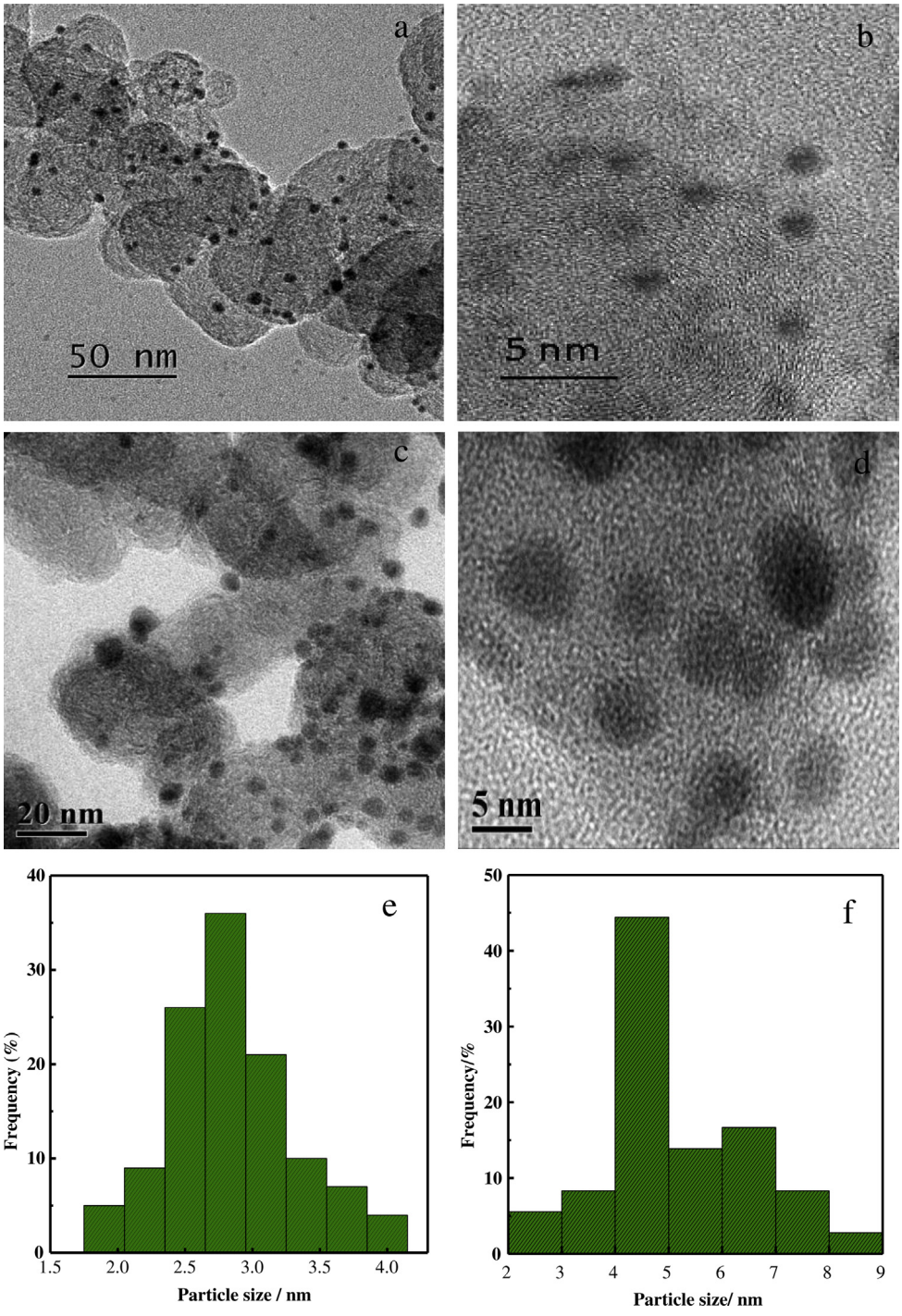

Fig. 2. TEM images and the corresponding particle size distribution column diagrams of AuPt/C (a, b, e) and AuPt@Pd/C-b (c, d, f).

The diffraction peak for AuPt@Pd/C has a negative shift (about 1.7°) compared to pure Pd/C, and in accordance with AuPt/C, which further confirms that Pd was deposited on the surface of the AuPt alloy particles instead of forming independent nanoparticles.

Fig. 2 presents the TEM images of AuPt/C and AuPt@Pd/C, which show that the active components on the carbon supports are uniformly dispersed. Although it is difficult to observe the core–shell structure of AuPt@Pd/C directly using TEM, some important information about AuPt@Pd can be obtained by the TEM analysis. We measured the distribution of the AuPt and AuPt@Pd nanoparticles and found that the average particle sizes of AuPt/C and AuPt@Pd/C were 2.8 nm and 4.9 nm respectively, which seems quite consistent with the particle results observed by XRD. The increase in particle size may have arisen from the coverage of Pd on the AuPt core nanoparticles; in other words, these results can be viewed as confirming the core–shell structure of the AuPt@Pd/C catalyst.

CO_{ad} stripping voltammograms of AuPt@Pd/C in 0.5 M H_2SO_4 solution are presented in Fig. 3. Generally, Au atoms only adsorb a negligible amount of CO_{ad} compared with Pt [28], a fact supported by our results showed in Fig. 3, where almost no CO_{ad} stripping peak appears on the voltammogram of Au/C. All the CO_{ad} oxidation peaks observed for AuPt/C can be assigned to the existence of Pt atoms. The CO_{ad} stripping voltammograms of AuPt/C and Pd/C indicated that the stripping peaks of CO_{ad} at 0.54 V and 0.8 V belong to the oxidation of CO_{ad} on Pt and Pd respectively. The adsorption area of CO_{ad} on Pt was determined by integrating the charge of the electrodesorption peak of adsorbed CO_{ad} on Pt. The results normalized by the mass of Pt are 12.04 $m^2\ g^{-1}$ and 11.28 $m^2\ g^{-1}$ for AuPt/C and AuPt@Pd/C, respectively. The decrease in adsorption peak of CO on AuPt/C seems indicate that the AuPt nanoparticles have been partially coated by a Pd shell, but not completely. The obviously lower onset oxidation potential of the AuPt@Pd/C catalyst is an indication of that CO_{ad} is easily oxidized on AuPt@Pd/C, which may be due to the synergic effect between Au or Pt in the core and the Pd shell atoms.

To obtain information about the surface composition, the surface electronic structure of the AuPt@Pd/C catalyst was further evaluated by X-ray photoelectron spectroscopy (XPS). Fig. 4a shows the wide-scan XPS spectra of AuPt@Pd/C. The detected content ratio of Pd to Au in the surface of nanoparticles is obviously higher than that in the bulk nanoparticles as measured by atomic absorption spectroscopy, demonstrating that the surface of AuPt@Pd/C is enriched by Pd, which is possibly an indication of Pd covering the AuPt nanoparticles. Fig. 4b and c shows the detailed XPS spectra of Au 4f and Pd 3d in AuPt@Pd/C. Each spectrum was analyzed by deconvolution method, after which the peaks with binding energies of 84.45 eV and 88.14 eV were ascribed to Au, both peaks move positively when compared with what has been reported in the literature [29,30]. Regarding the binding energy of Pd 3d, it was found that the binding energies of Pd (341.71 eV and 336.40 eV) of the AuPt@Pd/C are higher those of the commercial Pd/C (340.96 eV and 335.65 eV) (see Fig. 4e). The positive shifts of binding energies of both Au and Pd may result from the interaction between the Au in core and Pd in the surface of the prepared core–shell AuPt@Pd/C, which indicates that Pd was deposited on the surface of the metal core nanoparticles rather than on the carbon.

We investigated the effect of electrodeposition modes—non-pulse and pulse—on the catalysts' activities. Fig. 5 presents the hydrogen under-potential deposition (HUPD) of AuPt/C and AuPt@Pd/C. When the same amount of Pd was deposited onto AuPt/C, pulse electrodeposition yield a larger electrochemical catalytic surface area than non-pulse electrodeposition. Similarly, the AuPt@Pd/C prepared by pulse electrodeposition showed much higher catalytic activity towards the oxidation of formic acid than that prepared by non-pulse electrodeposition, as can be seen in Fig. 6. Therefore, we chose the pulse electrodeposition mode for the further research described in the remainder of this paper.

We also studied the effect of the ratio of T_{off} to T_{on} on the electrocatalytic activity of AuPt@Pd/C. We used the same deposition time to deposit the same volume of Pd, while varying the time of disconnection. The ratios of T_{off} to T_{on} were 1:1, 5:1 and 10:1. From the results shown in Figs. 7and 8, we can see that when the ratio was 5:1, the AuPt@Pd/C presented the largest electrochemical catalytic surface area and the highest electrocatalytic activity towards the oxidation of formic acid. This may be because with this time ratio, not only can the Pd^{2+} consumed during deposition be replenished, but the concentration polarization can be eliminated and the formation of hydrogen suppressed.

Cyclic voltammograms for AuPt@Pd/C catalysts with different Pd contents in N_2-saturated 0.5 M H_2SO_4 is presented in Fig. 9. We used the same T_{off} to T_{on} ratio (5:1) and different pulse numbers to prepare different AuPt@Pd/C catalysts. The theoretical ratios of Au to Pd were 40:1, 30:1, and 20:1 and we labeled the relevant catalysts AuPt@Pd/C-40, AuPt@Pd/C-30, and AuPt@Pd/C-20, respectively. The composition of the catalysts was measured by atomic adsorption spectrum and the data was presented in Table 1, it was found that the real Pd depositing amount is about ten times of theoretical amount. The number of Pd surface atoms was estimated from the charge associated with HUPD in the region about −0.14 V to 0 V, using the stoichiometry of one adsorbed H atom per Pd atom. From the results we could see that as the Pd content in AuPt@Pd/C grew, the area of HUPD increased, which also indicated the existence of Pd.

Fig. 10 describes the oxidation of formic acid on E-TEK Pd/C and AuPt@Pd/C catalysts with different amounts of Pd in a solution of 0.5 M H_2SO_4 + 0.5 M HCOOH at a scan rate of 50 mV s^{-1}. The Pd mass activities for the AuPt@Pd/C catalysts were 4.4 A $mg^{-1}{}_{Pd}$, 3.0 A $mg^{-1}{}_{Pd}$ and 2.7 A $mg^{-1}{}_{Pd}$ which were 8.5, 5.8 and 5.2 times that of E-TEK Pd/C. AuPt/C shows very low activity towards the oxidation of formic acid. However, after Pd was deposited, the activity level was greatly enhanced from 0.098 A $mg^{-1}{}_{metal}$ to 0.83 A $mg^{-1}{}_{metal}$, 0.73 A $mg^{-1}{}_{metal}$ and 0.83 A $mg^{-1}{}_{metal}$, indicating that Pd was coated on the surface of AuPt nanoparticles; this conclusion is also supported by the shape of the catalysts'

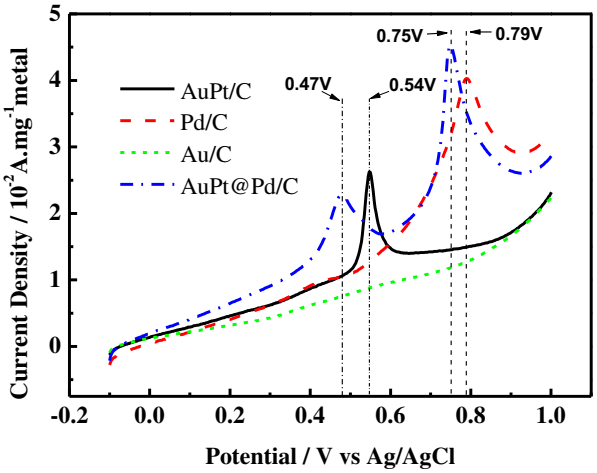

Fig. 3. CO stripping voltammograms of AuPt/C, Pd/C, Au/C, and AuPt@Pd/C in 0.5 M H_2SO_4 solution at room temperature and at a scan rate of 20 mV s^{-1}.

voltammograms, as the voltammograms of AuPt@Pd/C catalyst were very similar to those of Pd/C, but not to those of AuPt/C catalyst.

Even when whole metals were considered, the mass activity of AuPt@Pd/C also showed better activity than that of E-TEK Pd/C, the activity of the former being 1.6, 1.4 and 1.6 times that of the later.

We suggest that the remarkably higher activity of AuPt@Pd/C catalyst can be attributed to the high dispersion of Pd on the surface of AuPt nanoparticles, the synergic effect of the AuPt core and the Pd shell, as well as the electronic structure effect (strain and ligand effects) between the AuPt core and the Pd shell.

The stability of the catalysts was evaluated by chronoamperometry, the results of which are shown in Fig. 11. The currents of the AuPt@Pd/C catalysts rose a bit initially, indicating that the deposited Pd needed some time to activate, which was similar to the CV results. Moreover, during the whole procedure, all the AuPt@Pd/ catalysCts exhibited higher current densities than E-TEK Pd/C and among these, AuPt@Pd-40 showed the highest activity and stability.

4. Conclusion

In summary, a core–shell structured AuPt@Pd/C catalyst was successfully prepared using a pulse electrodeposition approach.

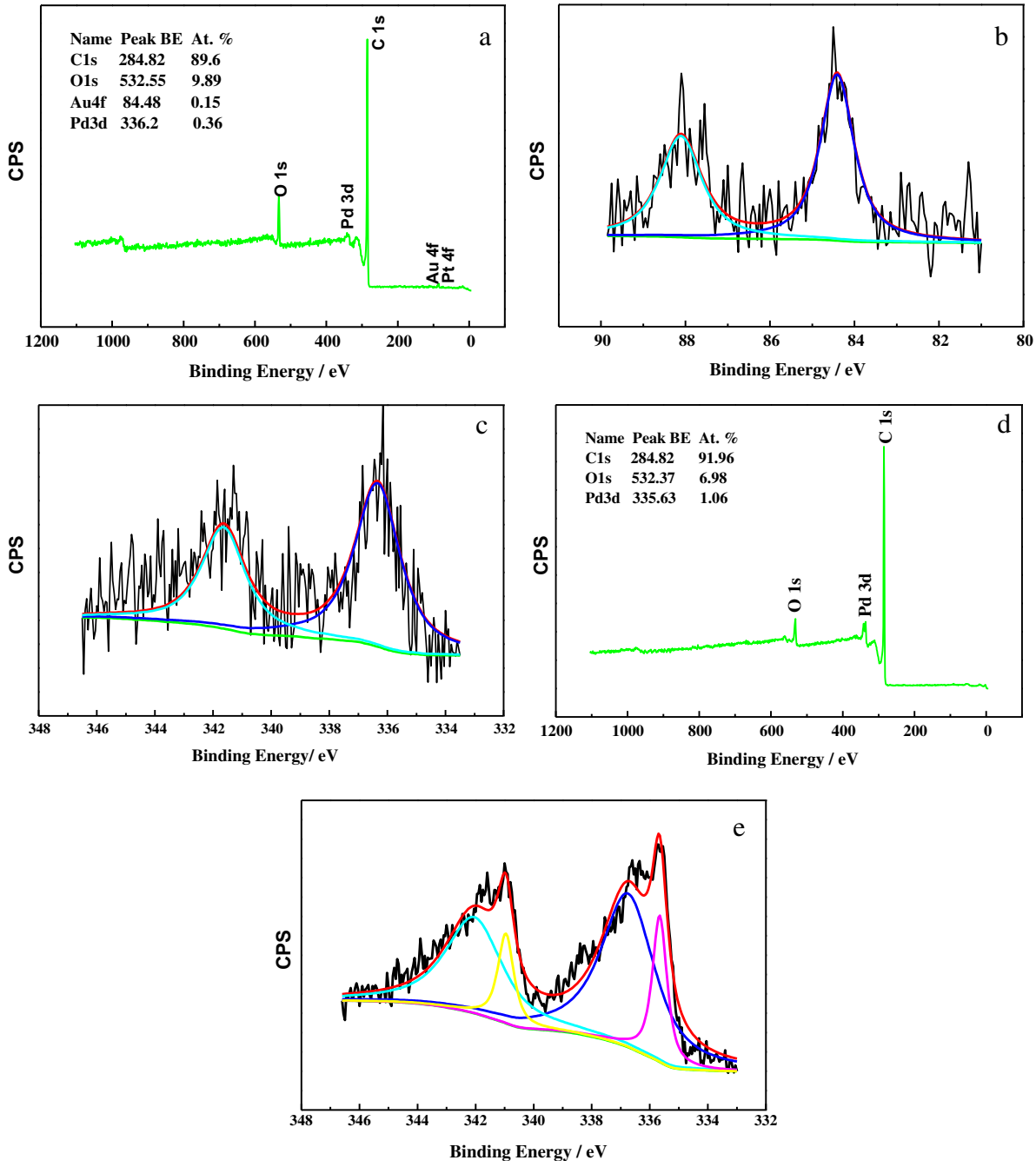

Fig. 4. Survey XPS spectra (a), Au 4f XPS spectra (b), Pd 3d XPS spectra (c) of AuPt@Pd/C and Survey XPS spectra (d) and Pd 3d XPS spectra (e) of commercial Pd/C.

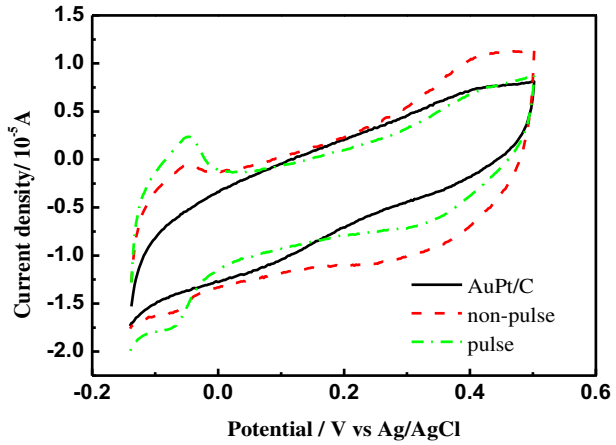

Fig. 5. Cyclic voltammograms of AuPt/C and AuPt@Pd/C in 0.5 M H_2SO_4 solution at room temperature and a scan rate of 50 mV s^{-1}.

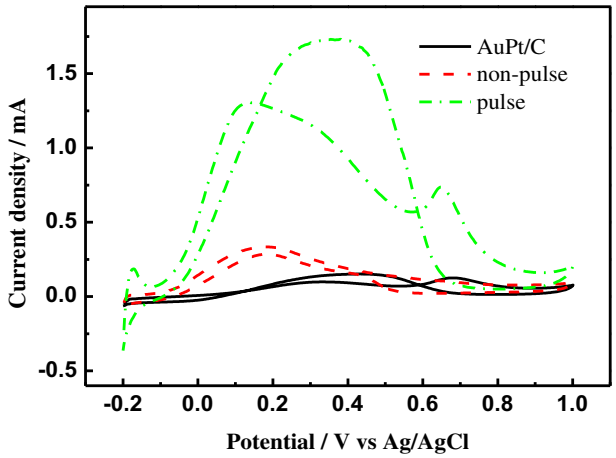

Fig. 6. Cyclic voltammograms of AuPt/C and AuPt@Pd/C in 0.5 M H_2SO_4 + 0.5 M HCOOH solution at room temperature and at a scan rate of 50 mV s^{-1}.

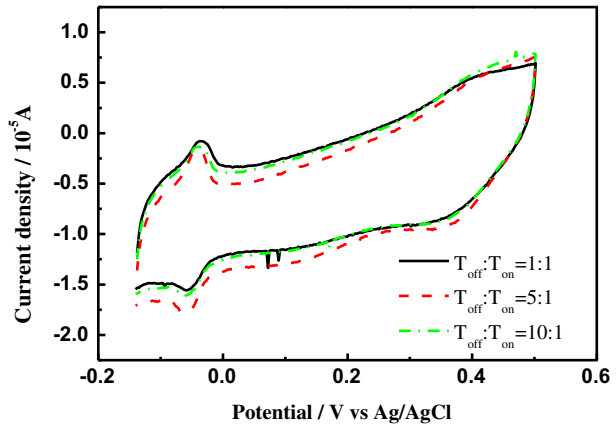

Fig. 7. Cyclic voltammograms of AuPt@Pd/C in 0.5 M H_2SO_4 solution at room temperature and a scan rate of 50 mV s^{-1}.

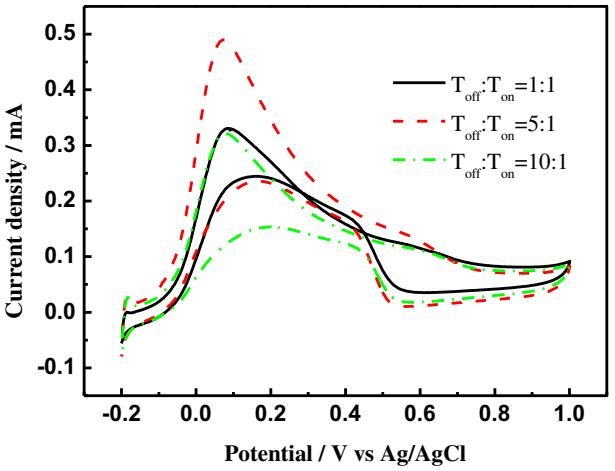

Fig. 8. Cyclic voltammograms of AuPt@Pd/C catalysts in 0.5 M H_2SO_4 + 0.5 M HCOOH solution at room temperature and a scan rate of 50 mV s^{-1}.

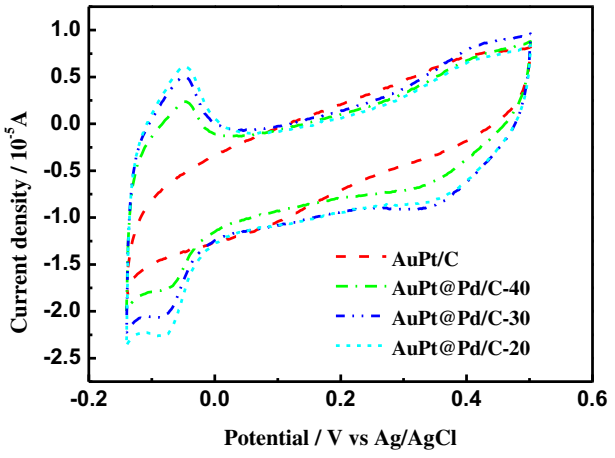

Fig. 9. Cyclic voltammograms of AuPt@Pd/Cs and Pd/C in 0.5 M H_2SO_4 solution at room temperature and at a scan rate of 50 mV s^{-1}.

The catalyst showed excellent activity towards the anodic oxidation of formic acid and its core–shell structure was revealed by TEM, XPS and XRD results. It should be pointed out that although the activity was greatly enhanced, the core elements used in this work—Au and Pt—are more costly than Pd. To reduce the cost and make the core–shell catalyst more commercially attractive for DFAFC, we will attempt to use lower cost cores in our future work that still maintain the Pd mass activity enhancements demonstrated here.

Table 1
The composition of AuPt@Pd/C catalysts measured by AAS.

Sample	Pd[a]	Au[a]	Pt[a]	n_{Pd}:n_{Au}:n_{Pt}[b]
AuPt@Pd/C-20	2.30%	4.88%	0.17%	1:1.15:0.04
AuPt@Pd/C-30	1.60%	4.91%	0.17%	1:1.66:0.06
AuPt@Pd/C-40	1.18%	4.93%	0.17%	1:2.26:0.08

[a] By weight.
[b] Atomic ratio.

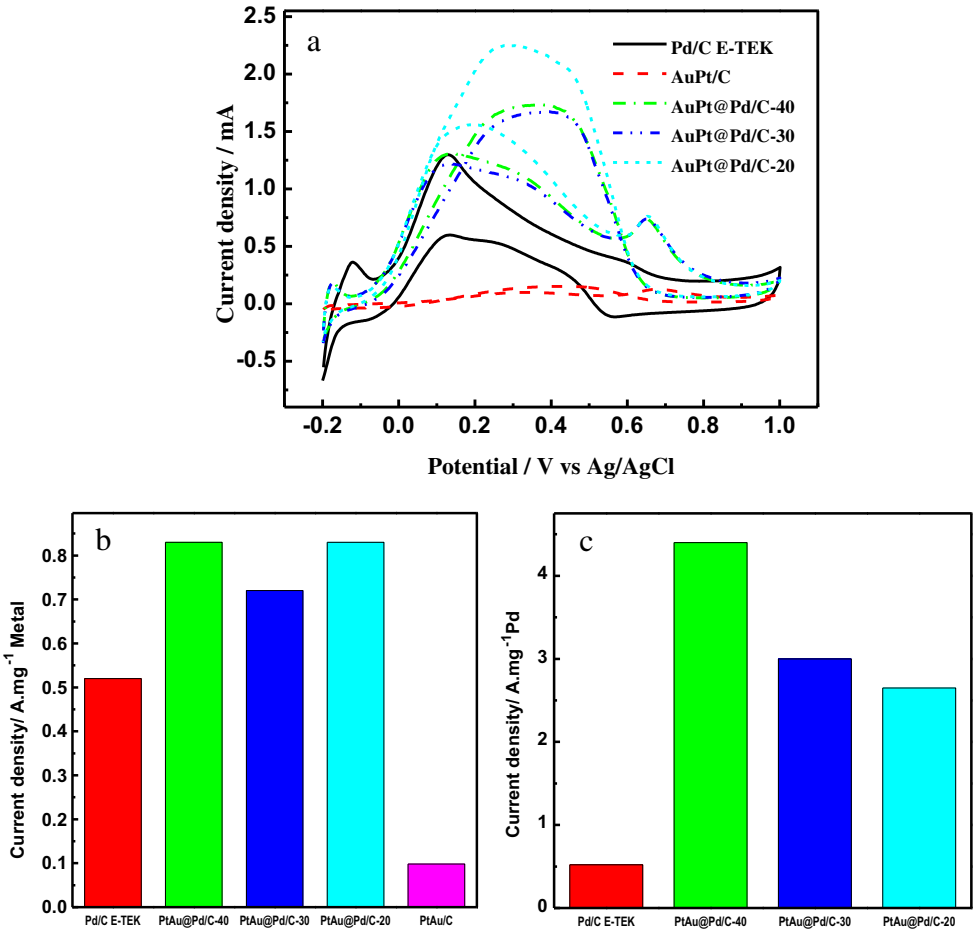

Fig. 10. Cyclic voltammograms (a) and corresponding column diagrams of mass activity of Pd/C, AuPt/C and AuPt@Pd/C for metals (b) and Pd (c) in 0.5 M H_2SO_4 + 0.5 M HCOOH solution at room temperature and at a scan rate of 50 mV s^{-1}.

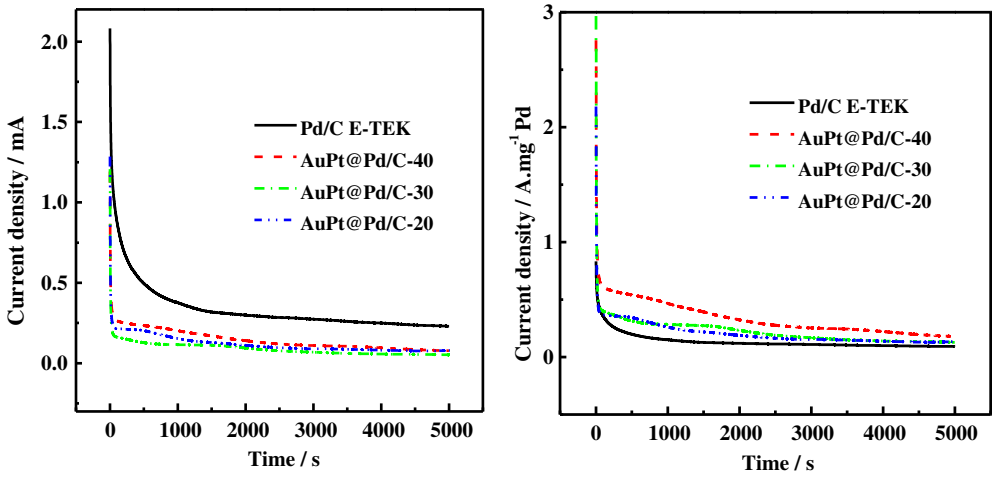

Fig. 11. Chronoamperometry and corresponding current densities of Pd/C and AuPt@Pd/C in 0.5 M H_2SO_4 + 0.5 M HCOOH solution at 0.1 V and a rate of 300 r s^{-1}.

Acknowledgments

The authors gratefully acknowledge the NSFC of China (Project Numbers 21276098 and 21076089) for financial support of this work.

References

[1] T.Y. Jeon, S.J. Yoo, H.Y. Park, S.K. Kim, S. Lim, D. Peck, D.H. Jung, Y.E. Sung, Langmuir 28 (2012) 3664–3670.

[2] C.H. Chen, W.J. Liou, H.M. Lin, S.H. Wu, A. Borodzinski, L. Stobinski, P. Kedzierzawski, Fuel Cells 10 (2010) 227–233.
[3] K.J. Jeong, C.M. Miesse, J.H. Choi, Journal of Power Sources 168 (2007) 119–125.
[4] F. Cheng, S.M. Kelly, N.A. Young, C.N. Hope, K. Beverley, M.G. Francesconi, S. Clark, J.S. Bradley, F. Lefebvre, Chemistry of Materials 18 (2006) 5996–6005.
[5] C. Rice, S. Ha, R.I. Masel, P. Waszczuk, A. Wieckowski, T. Barnard, Journal of Power Sources 111 (2002) 83–89.
[6] S. Uhm, H.J. Lee, Y. Kwon, J. Lee, Angewandte Chemie 47 (2008) 10163–10166.
[7] C. Rice, S. Ha, R.I. Masel, A. Wieckowski, Journal of Power Sources 115 (2003) 229–235.
[8] X.W. Yu, P.G. Pickup, Journal of Power Sources 182 (2008) 124–132.
[9] Y.H. Qin, J. Yue, H.H. Yang, X.S. Zhang, X.G. Zhou, L. Niu, W.K. Yuan, Journal of Power Sources 196 (2011) 4609–4612.
[10] Z. Liua, L. Hong, M.P. Thama, T.H. Lima, H. Jianga, Journal of Power Sources 161 (2006) 831–835.
[11] V. Mazumder, S. Sun, Journal of the American Chemical Society 131 (2009) 4588–4589.
[12] S.E. Habas, H. Lee, V. Radmilovic, G.A. Somorjai, P. Yang, Nature Materials 6 (2007) 692–697.
[13] W.P. Zhou, A. Lewera, R. Larsen, R.I. Masel, P.S. Bagus, A. Wieckowski, Journal of Physical Chemistry B 110 (2006) 13393–13398.
[14] N. Hoshi, K. Kida, M. Nakamura, M. Nakada, K. Osada, Journal of Physical Chemistry B 110 (2006) 12480–12484.
[15] R.K. Pandey, V. Lakshminarayanan, Journal of Physical Chemistry C 113 (2009) 21596–21603.
[16] Z.Z. Yin, J.J. Zhang, L.P. Jiang, J.J. Zhu, Journal of Physical Chemistry C 113 (2009) 16104–16109.
[17] J. Yu, R.B. Zhang, W.Z. Pan, L. Schimansky-Geier, Physica Scripta 78 (2008).
[18] F.K. Cheng, C. He, D. Shu, H.Y. Chen, J. Zhang, S.Q. Tang, D.E. Finlow, Materials Chemistry and Physics 131 (2011) 268–273.
[19] H. Meng, S. Sun, J.P. Masse, J.P. Dodelet, Chemistry of Materials 20 (2008) 6998–7002.
[20] Xin Wang, Yawen Tang, Ying Gao, T. Lu, Journal of Power Sources 175 (2008) 784–788.
[21] H.X. Zhang, C. Wang, J.Y. Wang, J.J. Zhai, W.B. Cai, Journal of Physical Chemistry C 114 (2010) 6446–6451.
[22] S. Zhang, M. Qing, H. Zhang, Y. Tian, Electrochemistry Communications 11 (2009) 2249–2252.
[23] H.L. Gao, S.J. Liao, J.H. Zeng, Y.C. Xie, D. Dang, Electrochimica Acta 56 (2011) 2024–2030.
[24] Y.N. Wu, S.J. Liao, H.F. Guo, X.Y. Hao, Journal of Power Sources 224 (2013) 66–71.
[25] Y.J. Kang, L. Qi, M. Li, R.E. Diaz, D. Su, R.R. Adzic, E. Stach, J. Li, C.B. Murray, ACS Nano 6 (2012) 2818–2825.
[26] S. Zhang, Y.Y. Shao, G.P. Yin, Y.H. Lin, Angewandte Chemie International Edition 49 (2010) 2211–2214.
[27] Z.X. Liang, T.S. Zhao, Journal of Physical Chemistry C 111 (2007) 8128–8134.
[28] Y. Yu, K.H. Lim, J.Y. Wang, X. Wang, Journal of Physical Chemistry C 116 (2011) 3851–3856.
[29] T.D. Thomas, P. Weightman, Physical Review B 33 (1986) 5406–5413.
[30] M.T. Anthony, M.P. Seah, Surface and Interface Analysis 6 (1984) 95–106.